



Growth or decay of a coherent structure interacting with random waves

Yuanting Chen  and Benno Rumpf ^{*}

Department of Mathematics, Southern Methodist University, Dallas, Texas 75205, USA



(Received 2 June 2021; accepted 18 August 2021; published 15 September 2021)

Solitary waves interacting with random Rayleigh-Jeans distributed waves of a nonintegrable and noncollapsing nonlinear Schrödinger equation are studied. Two opposing types of dynamics are identified: First, the random thermal waves can erode the solitary wave; second, this structure can grow as a result of this interaction. These two types of behavior depend on a dynamical property of the solitary wave (its angular frequency), and on a statistical property of the thermal waves (the chemical potential). These two quantities are equal at a saddle point of the entropy that marks a transition between the two types of dynamics: high-amplitude coherent structures whose frequency exceeds the chemical potential grow and smaller structures with a lower frequency decay. Either process leads to an increase of the wave entropy. We show this using a thermodynamic model of two coupled subsystems, one representing the solitary wave and one for the thermal waves. Numerical simulations verify our results.

DOI: [10.1103/PhysRevE.104.034213](https://doi.org/10.1103/PhysRevE.104.034213)

I. INTRODUCTION

The dynamics of nonlinear waves of fluids [1–3], Bose-Einstein condensates [4], plasmas [5], and light interacting with matter [6,7] generates in certain circumstances coherent high-amplitude structures that emerge spontaneously from a weakly nonlinear background of disordered waves. In this paper, we give a statistical analysis of a solitary wave interacting with random thermal waves. We show and explain in detail that this coherent structure can either be eroded by the surrounding random waves (Fig. 1) or it can grow by this interaction (Fig. 2). Which of the two processes occurs depends on the size of the solitary wave and the statistical properties of the disordered waves.

The equation of motion under investigation [8,9] is a generic nonintegrable Hamiltonian system, namely, the vari-

$$i \frac{\partial \phi}{\partial t} = \frac{\partial^2 \phi}{\partial x^2} + |\phi|^2 \phi - |\phi|^4 \phi \quad (1)$$

of the focusing nonlinear Schrödinger equation for a complex field $\phi(x, t)$. While our main result is applicable to arbitrary dimensions, we study the system in one spatial dimension. The quintic order term eliminates most conservation laws that the cubic nonlinear Schrödinger equation has while its sign ensures saturation of soliton amplitudes. This six-wave interaction term is (unlike the trivial four-wave interaction) not removable by a canonical transformation and it contributes to energy transfer between modes [7]. It is obtained as the next order term of phase-symmetric nonlinearities, e.g., of the saturated nonlinearity $\phi|\phi|^2/(1+|\phi|^2)$. Equation (1) is equivalent to an equation

$$i \frac{\partial \psi}{\partial T} = D \frac{\partial^2 \psi}{\partial X^2} + c_3 |\psi|^2 \psi - c_5 |\psi|^4 \psi,$$

with arbitrary real positive coefficients D, c_3, c_5 via the scaling transformation $\psi(X, T) = A\phi(x, t)$ with $A = \sqrt{c_3/c_5}$, $x = c_3 X / \sqrt{c_5 D}$, $t = c_3^2 T / c_5$ and multiplication of the equation by $\sqrt{c_5^3/c_3^5}$. More generally, positive or negative factors D, c_3, c_5 yield four basic types of equations with the nonlinearities $\pm|\phi|^2\phi \pm |\phi|^4\phi$.

Equation (1) derives as $i\dot{\phi} = -\frac{\delta\mathcal{H}}{\delta\phi^*}$ from the Hamiltonian

$$\mathcal{H}[\phi, \phi^*] = \int_0^L (|\phi_x|^2 - \frac{1}{2}|\phi|^4 + \frac{1}{3}|\phi|^6) dx, \quad (2)$$

other conserved quantities that are the wave action

$$\mathcal{A}[\phi, \phi^*] = \int_0^L |\phi|^2 dx \quad (3)$$

(associated to the phase symmetry) and the momentum $\mathcal{P}[\phi, \phi^*] = i \int_0^L (\phi_x \phi^* - \phi \phi_x^*) dx$ (associated to the translational symmetry). L is the system size, the boundary conditions are periodic. We denote the fixed values as $\mathcal{H} = E$ (energy) and $\mathcal{A} = A$, and we only consider a zero momentum $\mathcal{P} = 0$. A/L being small ensures that the amplitude $|\phi|$ is small at least almost everywhere in real space.

Deferring details to the Secs. II and III, we now outline the main features of the simulations of Figs. 1 and 2. Equation (1) with a system size $L = 4096$ and periodic boundary conditions is integrated in time. The initial conditions of both simulations comprise the same solitary wave which has a squared amplitude $|\phi_m|^2 = 0.238$ and a frequency $\omega_s = -0.1$; its momentum is zero. The surrounding waves are Rayleigh-Jeans distributed with a high-wave number cutoff that reduces aliasing errors. Conjugate to the two conserved quantities \mathcal{H} and \mathcal{A} are the inverse temperature β (that measures the rate of change of the entropy under changes of the energy) and the chemical potential μ (related to the rate of change of the entropy under changes of the wave action). The thermal waves in the simulation of Fig. 1 initially have a chemical potential

^{*}brumpf@smu.edu

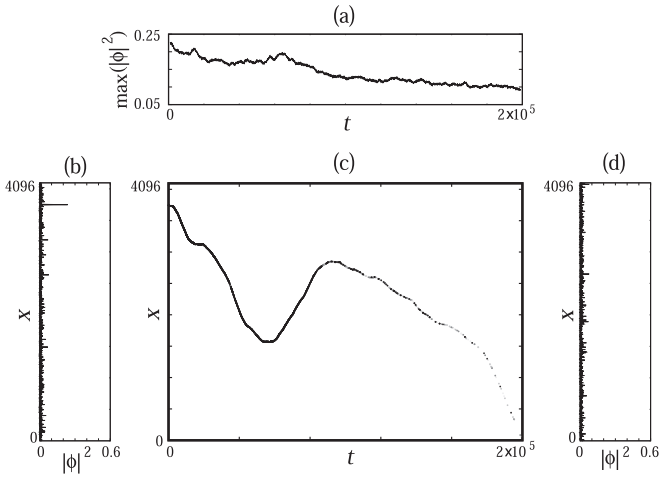


FIG. 1. Decay of a solitary wave interacting with thermal waves. Equation (1) is integrated over 2×10^5 time units. The initial state contains a solitary wave with a frequency $\omega_s = -0.1$ and an amplitude $|\phi_m|^2 \approx 0.238$. It is immersed in thermal waves with a chemical potential $\mu = -0.2$; the average amplitude is $\langle |\phi|^2 \rangle \approx 0.008$. The system size is $L = 4096$ with periodic boundary conditions. $x = 0$ in this plot is arbitrarily set in a way that the boundary $x = 0$ or $x = 4096$ is not crossed by the solitary wave in this particular simulation. (a) Time evolution (moving average over 2000 time units) of the spatial maximum of $|\phi|^2$. The solitary wave decays from its initial amplitude $|\phi|^2 \approx 0.238$ below the amplitude of the background waves. (b) Initial amplitude profile $|\phi(x, t = 0)|^2$ at the starting point of the simulation; the solitary wave is located near $x = 4000$. (c) Locations with $|\phi(x, t)|^2 \geq 0.16$ tracing the decaying solitary wave in space and time. (d) Amplitude profile $|\phi(x, t = 2 \times 10^5)|^2$ at the end point of the simulation, the solitary wave is indistinguishable from the surrounding waves.

$\mu = -0.2$ (i.e., $\mu < \omega_s < 0$), in Fig. 2, it is $\mu = -0.05$ (i.e., $\omega_s < \mu < 0$). The temperatures of the waves are chosen such that the average wave action $\langle |\phi|^2 \rangle = 0.008$ is the same in the two simulations.

We find that thermal waves with $\mu < \omega_s$ in the simulation of Fig. 1 erode of the solitary wave so its amplitude decays and it becomes indistinguishable from the background thermal waves. Thermal waves with $\mu > \omega_s$ in the simulation of Fig. 2 cause a growth of the solitary wave. This threshold between decay and growth at $\mu = \omega_s$ is found persistently in various simulations, including varying temperatures, frequencies, and chemical potentials. This type of transition has previously been found in a nonlinear lattice [10], which among other differences can have positive and negative temperatures. Our aim is to explain the threshold between growth and decay and the ensuing stable states. In Sec. II, we introduce a statistical model by dividing the system into a subsystem that contains one solitary wave (Sec. II A) and a subsystem of small-amplitude thermal waves (Sec. II B). The coupling of thermal waves and the solitary wave is described thermodynamically by its effect on the equilibrium entropy of the two systems (Sec. II C). We verify our results numerically in Sec. III. We finally discuss the applicability of these results for changed statistical properties of the random waves, higher dimensions, and the role of the momentum.

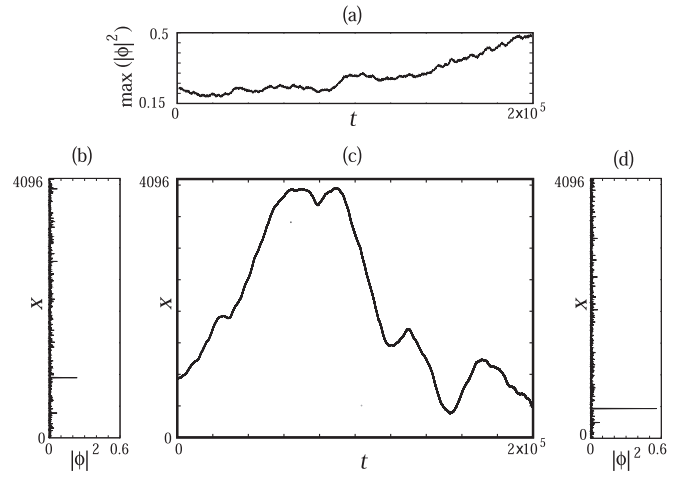


FIG. 2. Growth of a solitary wave interacting with thermal waves. The thermal waves have a chemical potential $\mu = -0.05$, everything else corresponds to Fig. 1. The solitary wave is initially located at $x \approx 1000$. Its amplitude grows during time evolution, it is $|\phi|^2 \approx 0.5$ at $t = 2 \times 10^5$.

II. STATISTICAL MECHANICS OF WAVES INTERACTING WITH A SOLITON: A MODEL OF TWO COUPLED COMPONENTS

A. Energy of nontraveling solitary waves

We first discuss some basic properties of solitary waves $\phi(x, t) = \phi_s(x, t)$ of Eq. (1). The Hamiltonian (2) under the constraint of a fixed wave action $\mathcal{A} = A_s$ is bounded from below; the minimal energy $\mathcal{H} = E_s(A_s)$ is achieved for solitary waves that follow from the variation $\delta(\mathcal{H} - \omega_s \mathcal{A}) = 0$ with a multiplier ω_s . The variation yields $\phi_{xx} + |\phi|^2 \phi - |\phi|^4 \phi = -\omega_s \phi$, which is associated to solutions $\phi_s(x, t) = e^{i\omega_s t} u(x)$ of (1); the frequency is given by the multiplier $\omega_s = dE_s/dA_s$. The real amplitude $u(x)$ is governed by the equation $u_{xx} = -\omega_s u - u^3 + u^5 = -\partial V/\partial u$ of a mass in a potential

$$V(u) = \frac{\omega_s}{2} u^2 + \frac{1}{4} u^4 - \frac{1}{6} u^6. \quad (4)$$

The wave action is finite if the waves are solitary, i.e., $u(x)$ decays to zero quickly enough for $x \rightarrow \pm\infty$. Such waves correspond to homoclinic orbits that connect the saddle point $u_1 = 0$ to itself. The potential $V(u)$ has a minimum at $u_2 > 0$ and a maximum at $u_3 > u_2$ if $-1/4 < \omega_s < 0$. For $-3/16 < \omega_s < 0$, this maximum has a positive value $V(u_3) > 0$ [Fig. 3(a)] so homoclinic orbits with an amplitude $u_m < \sqrt{3}/2$, $V(u_m) = 0$ exist [Fig. 3(b)]. For $\omega_s = -3/16$, the potential has the two maxima $V(u_1 = 0) = V(u_3 = \sqrt{3}/2) = 0$, a pair of heteroclinic orbits connecting them corresponds to domain walls between the domains $u_1 = 0$ for $x \rightarrow \mp\infty$ and $u_3 = u_m = \sqrt{3}/2$ at $x \rightarrow \pm\infty$. All these localized structures are nontraveling; traveling solitary waves have higher energies as they correspond to extrema of the Hamiltonian with the additional constraint by a nonzero momentum P .

The analytical expression of the solitary wave of (1) is [8,9]

$$u^2(x) = -\frac{12\omega_s}{3 + \sqrt{9 + 48\omega_s(2 \cosh^2(\sqrt{-\omega_s}x) - 1)}},$$

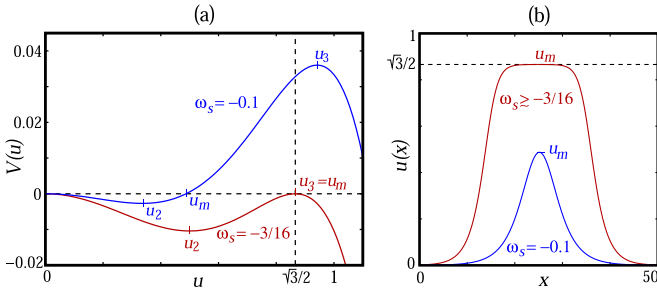


FIG. 3. (a) Potential $V(u)$ (4) for $\omega_s = -0.1$ and for $\omega_s = -3/16$. (b) Homoclinic orbits $u(x)$, $u_{xx} = -dV/du$ of the saddle point at $u_1 = 0$ for $\omega_s = -0.1$ and for $\omega_s \gtrsim -3/16$. The homoclinic orbit for $\omega_s = -0.1$ corresponds to a nontraveling solitary wave with a shape similar to the soliton of the focusing nonlinear Schrödinger equation. The homoclinic orbit for $\omega_s \gtrsim -3/16$ corresponds to a nontraveling solitary wave with a broad plateau at its maximum.

the energy and frequency are [8]

$$E_s(A_s) = \frac{3}{16}(\sqrt{3} \tanh\left(\frac{A_s}{\sqrt{3}}\right) - A_s) \quad (5)$$

and

$$\omega_s = \frac{dE_s(A_s)}{dA_s} = -\frac{3}{16} \tanh^2\left(\frac{A_s}{\sqrt{3}}\right) \quad (6)$$

(Fig. 4). In the limit of small A_s with $0 < -\omega_s \ll 3/16$, the quintic term is negligible and the solitary wave matches the soliton $u(x) = \sqrt{-2\omega_s} \operatorname{sech}(\sqrt{-\omega_s}x)$ of the focusing nonlinear Schrödinger equation with the energy $E_s \approx -A_s^3/48$ and $\omega_s \approx -3A_s^2/16$.

For $\omega_s \gtrsim -3/16$, the amplitude u_m of the homoclinic orbit is close to u_3 . The solitary wave has a broad plateau with $u(x) \lesssim \sqrt{3}/2$ [Fig. 3(b)] and a width Δx that diverges to infinity for $\omega_s \rightarrow -3/16$. The energy of the walls $\int_0^L |\phi_x|^2 dx$ is negligible for a broad solitary wave. The bulk energy scales

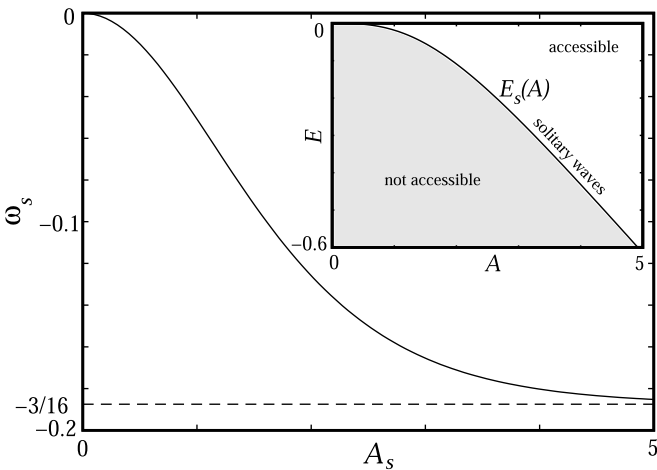


FIG. 4. Frequency $\omega_s(A_s) = dE_s(A_s)/dA_s$ (6) of solitary waves. Inset: Lower boundary $E_s(A)$ (5) of the Hamiltonian, points on the line correspond to nontraveling solitary waves. Any other states (traveling solitary waves, spatially extended waves, etc.) correspond to points above this line. The Hamiltonian cannot have values in the shaded area below this line.

as $E_s \approx (-u_3^4/2 + u_3^6/3)\Delta x = -9\Delta x/64$ and the bulk wave action as $A_s \approx u_3^2\Delta x = 3\Delta x/4$, so $E_s \approx -3A_s/16$ (Fig. 4).

A solitary wave may be represented by a nonlinear oscillator with $E_s(A)$ (5) being a Hamiltonian where A and α are action-angle variables. The canonical equations are $\dot{\alpha} = -\partial E_s(A)/\partial A = \omega_s$ and $\dot{A} = \partial E_s(A)/\partial \alpha = 0$. The microcanonical partition function (written with the Dirac- δ) is $\Omega_s = \int_0^{2\pi} \int_0^\infty \delta(E_s(A) - E_s(A_s)) dA d\alpha = 2\pi/|\partial E_s(A_s)/\partial A_s| = 2\pi/|\omega_s|$; the translational degree of freedom yields the system size as an irrelevant factor of this number. Notwithstanding the fact that this single oscillator system is far from the thermodynamic limit, we introduce an entropy $\ln \Omega_s = -\ln |\omega_s| + \text{const}$, which decreases as a function of $|\omega_s|$ and increases as a function of the energy E_s . Of course, this entropy is extremely small as it is associated to one degree of freedom only. The corresponding temperature,

$$\beta_s^{-1} = -\left(\frac{\partial E_s}{\partial A_s}\right)^2 / \frac{\partial^2 E_s}{\partial A_s^2} = \frac{3\sqrt{3}}{32} \sinh^2\left(\frac{A_s}{\sqrt{3}}\right) \tanh\left(\frac{A_s}{\sqrt{3}}\right),$$

is positive and grows as a function of A_s ; for small amplitudes, it behaves as $\beta_s^{-1} \approx A_s^3/32$.

B. Statistical mechanics of linear waves

We now review the basics of thermally distributed waves $\phi(x, t) = \phi_w(x, t)$ of (1). For $A/L \ll 1$ the amplitude is small almost everywhere. This suggests describing the small-amplitude part of the system with a Hamiltonian $\mathcal{H}_2[\phi, \phi^*] = \int_0^L |\phi_x|^2 dx$. The nonlinearity is taken into account only as a weak interaction between modes that allows the waves to thermalize.

Waves with a small amplitude $\phi_w = \sum a_k e^{ikx}$ can be described by the linear approximation $a_k \sim e^{i\omega_k t}$ with the frequencies $\omega_k = k^2$. Thermalization maximizes the wave entropy $S = \sum \ln n_k$ with $n_k = \langle |a_k|^2 \rangle$. The extremum of the wave entropy under the constraint of fixed energy $E_w = \sum \omega_k n_k$ and wave action $A_w = \sum n_k$ with multipliers β and μ ,

$$\delta(S - \beta(E_w - \mu A_w)) = 0,$$

yields the Rayleigh-Jeans distribution

$$n_k = \beta^{-1}(\omega_k - \mu)^{-1};$$

$n_k > 0$ requires $\mu < 0$.

The second variation of the constrained wave entropy,

$$\delta^2(S - \beta \sum (\omega_k - \mu) n_k) = -\frac{1}{2} \beta^2 \sum (\omega_k - \mu)^2 \delta n_k^2,$$

is negative, the Rayleigh-Jeans distribution is the maximum of the entropy under variations that redistribute the wave action among modes in a way that keeps the total wave action and energy constant.

As a general feature of the classical equilibrium statistics of continuous dynamical systems, the energy $E_w = \sum \omega_k n_k$ diverges for a canonical or grandcanonical ensemble where $\beta^{-1} \neq 0$ and possibly also μ are fixed. In other words, if the wave system is coupled to an infinite reservoir of energy and wave action, modes that are associated to infinitesimal wave lengths absorb an infinite amount of energy from the reservoir. For a microcanonical ensemble (energy and wave action of the

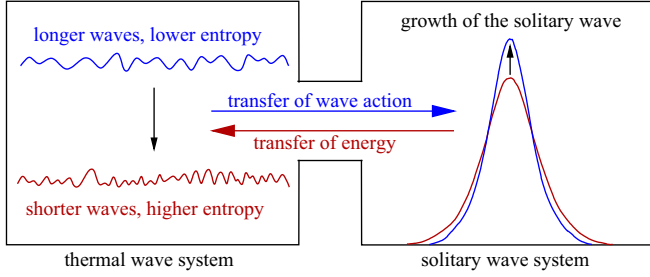


FIG. 5. Thermodynamic model: The dynamical coupling of a solitary wave and thermal waves is reduced to a thermodynamic coupling that enables the transfer of energy and wave action between the two systems. The sketch shows a growth process of the solitary wave: Wave action is transferred from the thermal waves to the solitary wave, energy is transferred in the opposite direction. Flows of each conserved quantity in the opposite direction lead to a decreasing solitary wave. Which of the two processes occurs depends on whether the flow of energy or of wave action has a greater entropic effect, which in turn depends on the chemical potential μ of the thermal waves and the frequency ω_s of the solitary wave.

waves are fixed), the energy spreads out over all modes, which each absorb only an infinitesimal amount of these quantities. To avoid such ultraviolet divergences, we introduce a finite cutoff wave number k_{\max} beyond which all degrees of freedom are ignored. In our numerical simulations in Sec. III, the initial wave action of waves beyond $|k_{\max}| = \pi/2$ is zero. The simulations show that spreading energy to higher wave numbers is a slow process compared to growth or decay of the solitary wave.

C. Thermal waves interacting with solitary waves

To represent the complete system (1), we now combine the solitary wave system ϕ_s and the thermal wave system ϕ_w . A dynamical description of the combined system involves the nonlinear coupling of the waves ϕ_s and ϕ_w . In the thermodynamics of the combined system, this coupling can be reflected by enabling a transfer of energy and wave action between the two subsystems (Fig. 5). Each subsystem is still described by its proper Hamiltonian (the quadratic approximation $\int_0^L |\phi_x|^2 dx$ for the thermal waves and the full Hamiltonian at its lower bound for the solitary wave). The sums $A_w + A_s = A$ and $E_w + E_s = E$ are conserved, growth or decay of the solitary wave correspond to transfers of these quantities. We consider the situation of the thermal waves being a large reservoir of wave action $A_w \gg A_s$ and energy $E_w \gg |E_s|$. Its temperature and chemical potential can be treated as being constant as long as the changes $|\Delta A_w/A_w|$, $|\Delta E_w/E_w|$ of the conserved quantities are small.

Whether the soliton grows or decays depends on the impact of these processes on the entropy of the small-amplitude thermal waves. The entropy of the solitary wave itself is neglected. The change of entropy $S(E_w, A_w)$ is

$$dS = \beta(dE_w - \mu dA_w). \quad (7)$$

Changes of the energy and wave action content of the solitary wave are connected by

$$dE_s - \omega_s dA_s = 0.$$

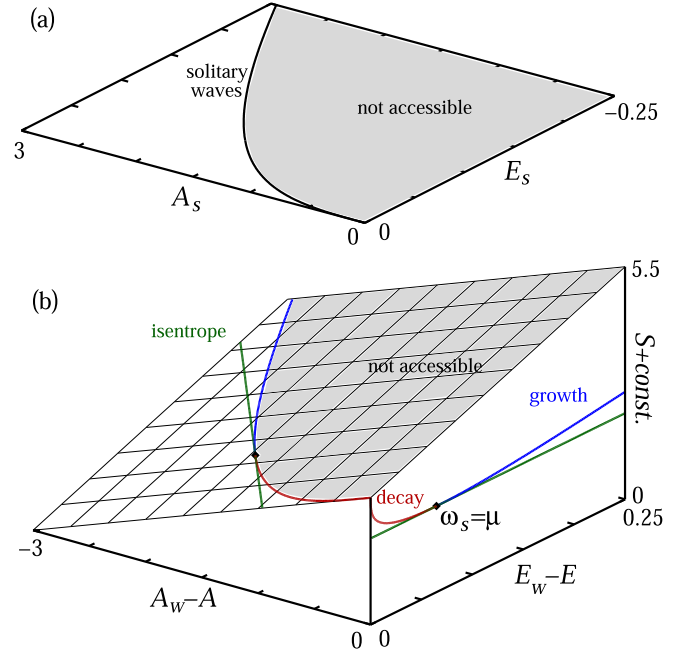


FIG. 6. (a) Lower boundary $E_s(A_s)$ of the Hamiltonian corresponding to the energy of solitary waves. (b) Wave entropy surface $S(A_w, E_w)$ of thermal waves for $\beta = 10$, $\mu = -0.1$. The green line is an isentrope $S = \text{const}$, with $dE_w/dA_w = \mu$. The energy and wave action of the thermal waves can change by transfers of these quantities from or to growing or decaying solitary waves. This corresponds to a time evolution along the boundary curve from (a) projected onto the entropy surface. Growth of large solitary wave ($\omega_s < \mu < 0$) increases the entropy (blue curve), while for small solitary wave ($\mu < \omega_s < 0$) it is decay that increases the entropy (red curve). The tangential point $\omega_s = \mu = -0.1$ corresponds to an unstable equilibrium of the solitary and the thermal waves.

With the conservation of total energy $dE_w + dE_s = 0$ and of wave action $dA_w + dA_s = 0$, the entropy can be expressed as a function $S(E_s(A_s), A_s)$ of the wave action of the solitary wave. Growth ($dA_s > 0$) or decay ($dA_s < 0$) of the solitary wave translates to entropy changes

$$dS = \beta(\mu - \omega_s)dA_s \quad (8)$$

of the thermal waves. At $\omega_s = \mu$, the wave entropy change vanishes in linear order (8), the quadratic order is

$$d^2S = -\beta \frac{d^2E_s}{dA_s^2} dA_s^2 > 0, \quad (9)$$

so this point is a minimum of the entropy with respect to growth or decay processes of the solitary wave.

Equation (8) gives the thermodynamic reason for growth or decay of the solitary waves. As a visualization of the entropy in the presence of a solitary wave, Fig. 6(a) shows the lower boundary $E_s(A_s)$ of the Hamiltonian, i.e., the energy of solitary waves. Energies in the shaded area beyond this line are inaccessible (compare Fig. 4). Figure 6(b) shows the entropy surface $S(E_w, A_w)$ of the thermal waves expressed as $S(E_w, A_w) = \beta(E_w - E - \mu(A_w - A)) + \text{const}$, with β and μ being constant. The conservation laws $E_w - E = -E_s$ and $A_w - A = -A_s$ project the energy boundary $E_s(A_s)$ of the

solitary energy of Fig. 6(a) to a boundary line $E_w(A_w)$ on the entropy surface of Fig. 6(b); it corresponds to the entropy of thermal waves that coexist with a solitary wave. The shaded region beyond that line (corresponding to a higher entropy) is again not accessible. The region below this line has by $\partial S/\partial E_w = \beta > 0$ and $\partial S/\partial A_w = -\beta\mu > 0$, a lower entropy under variations $dE_w < 0$ and $dA_w < 0$; in this region, a coherent wave whose energy is not extremal may coexist with thermal waves; entropy maximization pushes the coherent structure to the boundary. In other words, the solitary wave is stabilized by the thermodynamic forces β and μ .

We now discuss how the system can evolve along this boundary line. The isentrope $S(E_w, A_w) = \text{const}$, $dE_w/dA_w = \mu$ is tangential to the curve $E_w(A_w)$ at the point where $\omega_s = dE_s/dA_s = dE_w/dA_w = \mu$. This is the lowest entropy along the curve $E_w(A_w)$. In that sense, $\omega_s = \mu$ is a saddle point of the entropy. This point separates two regimes in which either growth or decay of the solitary wave leads to an increase of the entropy along the curve $E_w(A_w)$.

A solitary wave with smaller values A_s and $|E_s|$ will decrease when it interacts with the thermal waves: a gain of wave action $dA_w > 0$ increases the entropy of the thermal waves by $-\beta\mu dA_w$; at the same time, they lose energy $dE_w = \omega_s dA_w < 0$, which decreases their entropy by $\beta\omega_s dA_w$. By (8), the entropic effect of the transfer of wave action is bigger than the effect of the transfer of energy for $\mu < \omega_s < 0$. The solitary wave evolves along the red part of the curve $E_s(A_s)$ toward $A_s = 0$, $E_s = 0$ and, correspondingly, $E_w = E$, $A_w = A$.

A solitary wave with A_s and $|E_s|$ above the tangential point grows by interacting with the waves: It evolves along the blue part of curve $E_w(A_w)$, releases energy to the waves which increases their entropy; at the same time, this growth reduces the wave action of the thermal waves, but by (8) in this regime the entropic effect of the energy transfer is dominant. Two stages of growth can be distinguished: First, the amplitude and frequency ω_s of a smaller solitary wave with $|\omega_s| < 3/16$ grows as a function of A_s ; once the frequency approaches $|\omega_s| = 3/16$ its width grows as a function of A_s , while its amplitude and ω_s saturate. In an infinite system, the solitary wave is expected to grow indefinitely, in a large finite system, it will approach a two-phase equilibrium state, one low-amplitude phase, and one high-amplitude phase of the plateau of the solitary wave. This equilibrium is achieved by transferring enough energy and wave action so (at variance to the previous discussion) the chemical potential of the waves is not constant but approaches the same limit as ω_s .

III. NUMERICAL SIMULATIONS OF SOLITARY WAVES IMMERSED IN THERMAL WAVES

We verify the predictions of Sec. II by integrating (1) numerically with the same pseudospectral method as in Figs. 1 and 2. The nonlinearity is computed in real space and the time integration of (1) is carried out in Fourier space. The linear term $-k^2 a_k$ (corresponding to ϕ_{xx}) in the equations of motion for the Fourier modes a_k is removed by a transformation $b_k(t) = e^{-ik^2 t} a_k(t)$. The resulting nonstiff equations for \dot{b}_k are integrated in time using a multistep (Adams) method. The system size is $L = 2^{12}$ with periodic boundary conditions and with 2^{12} modes with wave numbers $-\pi < k \leq \pi$. The results

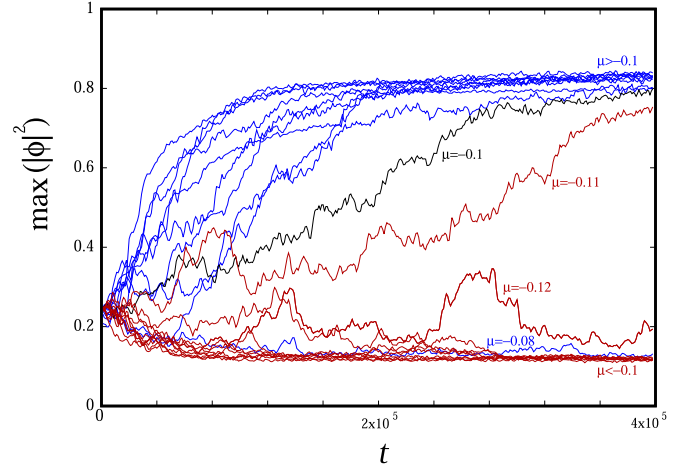


FIG. 7. Time evolution of the spatial maxima of $|\phi(x, t)|^2$ for a solitary wave with the initial frequency $\omega_s = -0.1$ and an initial squared amplitude $|\phi_m|^2 = 0.238$ (corresponding to the smaller solitary wave in Fig. 3) immersed in thermal waves with various temperatures and chemical potentials. The temperatures are chosen so the average squared amplitude is $\langle |\phi_w|^2 \rangle = 0.012$ for all simulations. The lines are running time averages over 2000 time units. The ten blue lines correspond to thermal waves with chemical potentials from $\mu = 0$ to $\mu = -0.09$, the black line corresponds to $\mu = -0.1$, and the ten red lines correspond to values from $\mu = -0.11$ to $\mu = -0.2$. Increase indicates growth of the solitary waves which approach the shape of the bigger structure in Fig. 3. Decrease indicates the erosion of the initial solitary waves which eventually decay below the amplitudes of the thermal waves.

are verified for larger ($L = 2^{14}$) system sizes and for various numerical accuracies. The weakness of the interaction of the solitary wave and the random waves requires relatively long and accurate integrations. The conservation of A is monitored as a measure for the numerical accuracy, where the relative error is $< 10^{-4}$ over the period of the numerical integration. The code has also been tested for solitary waves without noise and for soliton-soliton collisions for the integrable focusing nonlinear Schrödinger equation.

The initial condition is a state of one solitary wave that is immersed in but not covered by low-amplitude random waves. These waves have random phases, a Gaussian amplitude distribution and a Rayleigh-Jeans spectrum for $-\pi/2 \leq k \leq \pi/2$. Waves with $\pi/2 < |k| \leq \pi$ have zero amplitudes initially. Only a small amount of wave action flows into this region during the simulation, $|a_k|^2$ drops by at least two orders of magnitude at the cutoff. The spreading of energy to very short waves is a comparatively slow process.

Figures 7 and 8 give results for the same set of 21 numerical simulations for different chemical potentials which are varied from $\mu = -0.2$ to $\mu = 0$ with a step size 0.01. The temperature is adjusted so the average square amplitude of the background waves has the same value $\langle |\phi_w|^2 \rangle = 0.012$ for the initial conditions of all simulations; this makes the timescale of growth and decay processes for different values of μ more comparable without influencing the transition behavior. For $\mu = 0$, the wave action is gathered at $k = 0$. The solitary wave has initially a frequency $\omega_s = -0.1$ in each

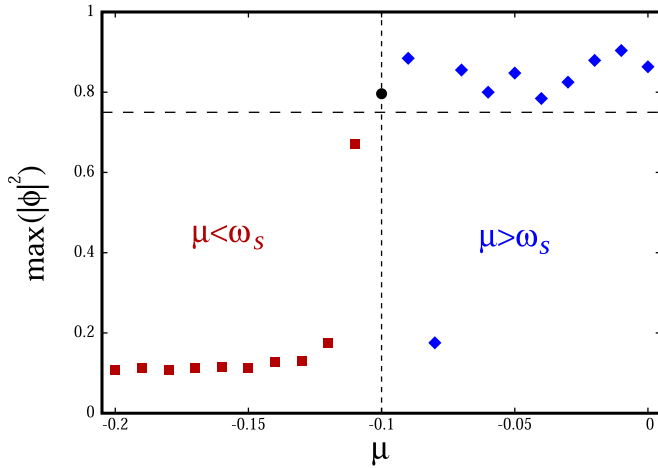


FIG. 8. Spatial maxima $\max(|\phi|^2)$ of the squared amplitude at $t = 4 \times 10^5$ for the simulations of Fig. 7. With the exception of outliers at $\mu = -0.11$ and $\mu = -0.08$, the solitary wave that has an initial frequency $\omega_s = -0.1$ grows and approaches the maximum amplitude $|\phi|^2 = 3/4$ for $-0.1 < \mu \leq 0$, and decays and vanishes in the background waves for $\mu < -0.1$.

simulation. About 4% of the total wave action is stored in the solitary wave and 96% is stored in the thermal waves for these initial conditions; the chemical potential and temperature change only slightly when the solitary wave is eroded.

Figure 7 shows the time evolution of the spatial maxima of $|\phi|^2$ for 21 runs, red branches correspond to $-0.2 \leq \mu < -0.1$, blue branches to $-0.1 < \mu \leq 0$, the black branch corresponds to $\mu = -0.1$. The end points of these simulations are plotted in Fig. 8 as a function of μ . We find that the solitary waves decay for $\mu < -0.1$, with the exception of the simulation with $\mu = -0.11$ in which it grows. Solitary waves with $-0.1 < \mu$ grow, with the exception of $\mu = -0.08$. Our simulations occasionally produce such outliers near the transition at $\mu = \omega_s = -0.1$. This is a consequence of the finite amplitude of the random waves that can push the initial solitary wave just above or below the threshold. Growing solitary waves develop a broad plateau similar to the bigger solitary wave in Fig. 3. Due to random-wave fluctuations, the maxima are slightly above the maximum $|\phi|^2 = 3/4$ of solitary waves. Decaying solitary waves decay below the level of the highest amplitudes of the random waves.

IV. DISCUSSION AND CONCLUSIONS

We now briefly discuss to what extent our results can be generalized. The distinctive property of solitary waves amid all other coherent structures is that they have the lowest possible energy for a given wave action. This makes solitary waves thermodynamically favorable, the thermodynamic forces β and μ push coherent structures toward the lower boundary of the Hamiltonian (Fig. 4). A solitary wave can evolve along this lower boundary of the Hamiltonian (Fig. 6). Small solitary structures decay when they interact with thermal waves if $\mu < \omega_s < 0$. In this case, the entropic effect of transferring wave action from the solitary wave to the thermal waves outweighs the entropic effect of the energy transfer in the opposite direction. The state of thermal waves without coherent

structures corresponds to a local maximum of the entropy. It is metastable in the statistical sense that it attracts almost all deviating states that are below a threshold; the deviations that are most favorable for growth are solitary waves for which the threshold is $\omega_s = \mu$. Escaping from the metastable state would require to decrease the wave entropy down to the saddle point of Fig. 6(b), which will occur only on extremely long timescales.

Large solitary waves with $\omega_s < \mu < 0$ grow as they interact with thermal waves. In this case, the entropic effect of an energy transfer to the thermal waves exceeds the effect of the flow of wave action in the opposite direction, which leads to a sustained growth of the coherent structure. The entropy resulting from this process ultimately exceeds the entropy of the small-amplitude state that corresponds to the point (0,0) in Fig. 6(b). In other words, the vast majority of microstates in the microcanonical ensemble contain a solitary wave [11]. In that sense, the small-amplitude phase is a marginal but physically relevant part of the microcanonical ensemble.

The regimes of growth and decay are separated by an unstable equilibrium state of a solitary wave and thermal waves with $\omega_s = \mu$. It corresponds to a tangent point $dE_s/dA_s = dE_w/dA_w|_{S=\text{const}}$ of an isentrope and the lower bound of the Hamiltonian in Fig. 6(b). The entropic effects of transfer of wave action and energy under growth or decay of the coherent structure cancel each other in linear order. By (9) with $d^2E_s/dA_s^2 < 0$, this is the minimum of the entropy (Fig. 6). At the same time, it is maximal with respect to variations $dA_s > 0$ with $dE_s = 0$ and $dE_s > 0$ with $dA_s = 0$, in that sense it is a saddle point. The assumption [12] that this is the maximum of entropy would be true for a coherent structure with the property $d^2E_s/dA_s^2 > 0$.

Our arguments are based only on the entropic effect of the allocation of the two conserved quantities to the random waves and the coherent structure. This is independent of the details of the interaction of the coherent structure and the random waves. Reference [13] discusses two dynamical processes for this; first, the direct interactions of solitary and small-amplitude waves, second, the interaction of a large solitary wave with smaller solitary waves. Such smaller solitary waves can emerge spontaneously from a modulational instability when $|\mu|$ is small and β^{-1} is sufficiently large. When such small solitary waves collide with a primary (and bigger) solitary wave, they transfer wave action to the bigger one while small amplitude waves are emitted [13,14]. The thermalization is then mediated by a gas of interacting solitary waves in which the largest structures gain an increasing amount of power.

The Hamiltonian corresponding to (1) in two and three dimensions is again bounded from below and supports circular or spherical solitary waves (minimizing the surface energy) with $E_s \gtrsim -3A_s/16$ as energy minima. Our statistical arguments can again be applied. The thermalization in two dimensions was studied in Ref. [8]: Starting from a modulational instability, droplets of the high-amplitude (or high-density liquid) phase and bubbles of a low-amplitude gas phase emerge and coalesce so the two phases become increasingly cohesive in a way similar to one-dimensional studies [13,14]. The coalescence of two droplets with the same

density is driven by the release of coupling energy from their boundaries that increases the wave entropy. Note that the fluctuations on top of the solitary waves provide a relevant entropy contribution if this high-amplitude phase fills a relevant part of the space.

Expressing our findings in this liquid-gas picture, the gas phase is metastable; droplets with a moderate density evaporate while droplets with a density above a critical threshold accumulate more particles which first leads to a further increase of the density, and subsequently a growth of the droplet size without further change of the density.

Our study did not involve nonzero momenta, and we observe only slow motions of the solitary wave caused by random interactions with the thermal waves. Nonzero momenta could be incorporated in both subsystems, which would lead to an additional balance of the speed of the solitary wave and a parameter v of the Rayleigh-Jeans distribution $n_k = 1/(\beta(\omega_k - vk - \mu))$. vk shifts the Rayleigh-Jeans distribution in wave-number space and absorbs some energy.

What is the physical status of classical thermal equilibria in Hamiltonian partial differential equations? For a canonical ensemble where the system is coupled to an external heat bath with a temperature β^{-1} , the infinitesimal-wavelength degrees of freedom absorb an infinite amount of energy. This was studied, e.g., in Ref. [15] for a fixed wave action. If energy and wave action are both fixed, the finite coupling energy is shared by all modes, so it flows to infinitesimal wavelengths [11]. The physical relevance of the attracting set is its influence on the dynamics at the scale where the wave equation is applicable. However, the spatial fluctuations on short (and certainly on infinitesimal) scales are outside the applicability of macroscopic wave equations, notably of envelope equations such as the nonlinear Schrödinger equation. Other effects such as the quantization of electromagnetic waves and viscosity of fluids are predominant at short scales. Our approach of a finite- k cutoff of n_k in the initial conditions is suitable for predicting growth and decay processes that occur at a shorter timescale than the spreading of energy towards short space scales. The cutoff can also have direct physical relevance: In photonics, a natural cutoff has been found as a result of higher-order dispersion terms that lead to truncated [16] or anomalous [17] thermalization, another effective cut-off can

be caused by proximity to the integrable case [18]. Finally, spatial discreteness of lattices confines the wave number to the Brillouin zone. Notably, the discrete nonlinear Schrödinger systems possess an additional transition between positive and negative temperatures [10,19–22].

With dissipation often superseding the wave dynamics at short scales, wave turbulence can emerge as a nonequilibrium state [1–3]. It can involve a direct cascade from long scales into the dissipation range and, if wave action is a second conserved quantity, and inverse cascade toward longer scales. This is generic in two or three dimensions as it requires nontrivial resonances of waves, but it has also been found in one dimension when the dispersion is suitably modified [23]. Kolmogorov-Zakharov distributed waves with $n_k \sim \omega_k^{-q}$; $q > 1$ can, in principle, support growth of coherent structures even more strongly than Rayleigh-Jeans distributed waves. The buildup of coherent structures is then a strongly nonlinear mechanism that feeds energy into the waves and that can coexist with the interaction of weakly correlated waves of turbulence [24]. The formation of localized structures can be a relevant contributor to dissipation [25].

To conclude, we have found either progressive growth or erosion of a coherent structure that interacts with random waves in a generic nonintegrable and noncollapsing nonlinear Schrödinger equation. Growth is at variance to wave collapses the result of an interaction with surrounding waves that supply wave action to the coherent structure. The erosion process drives the waves into a metastable low-amplitude thermal state. The threshold between growth and decay represents an unstable equilibrium that depends on a statistical property of the random waves (their chemical potential), and a dynamical property of the solitary wave (the angular frequency). The behavior that we have found is generic in the sense that it is a consequence of the entropy maximization under the constraints of conserved quantities; it can be expected to happen in various equations, dimensions, and types of spectra of the surrounding waves.

ACKNOWLEDGMENTS

This work was supported by a grant from the Simons Foundation (Grant No. 430192, B.R.).

- [1] A. C. Newell and B. Rumpf, *Annu. Rev. Fluid Mech.* **43**, 59 (2011).
- [2] V. E. Zakharov, V. L'vov, and G. Falkovich, *Kolmogorov Spectra of Turbulence* (Springer-Verlag, Berlin, 1992).
- [3] S. V. Nazarenko, *Wave Turbulence* (Springer-Verlag, Berlin, 2011).
- [4] C. Josserand, *C. R. Phys.* **5**, 77 (2004); R. Jordan and C. Josserand, *Phys. Rev. E* **61**, 1527 (2000).
- [5] E. A. Kuznetsov, A. M. Rubenchik, and V. E. Zakharov, *Phys. Rep.* **142**, 103 (1986).
- [6] A. Picozzi, J. Garnier, T. Hansson P. Suret S. Randoux, G. Millot, and D. N. Christodoulides, *Phys. Rep.* **542**, 1 (2014).
- [7] J. Laurie, U. Bortolozzo, S. Nazarenko, and S. Residori, *Phys. Rep.* **514**, 121 (2012).
- [8] C. Josserand and S. Rica, *Phys. Rev. Lett.* **78**, 1215 (1997).
- [9] M. M. Bogdan and A. S. Kovalev, *Pis'ma Zh. Eksp. Teor. Fiz.* **31**, 213 (1980) [*JETP Lett.* **31**, 195 (1980)].
- [10] B. Rumpf, *Europhys. Lett.* **78**, 26001 (2007); *Physica D (Amsterdam)* **238**, 2067 (2009).
- [11] R. Jordan, B. Turkington, and C. L. Zirbel, *Physica D (Amsterdam)* **137**, 353 (2000).
- [12] S. F. Krylov and V. V. Yankov, *Zh. Eksp. Teor. Fiz.* **79**, 82 (1980) [*Sov. Phys. JETP* **52**, 41 (1980)].
- [13] A. I. Dyachenko, V. E. Zakharov, A. N. Pushkarev, V. F. Shvets, and V. V. Yankov, *Zh. Eksp. Teor. Fiz.* **96**, 2026 (1988) [*Sov. Phys. JETP* **69**, 1144 (1989)].
- [14] V. E. Zakharov, A. N. Pushkarev, V. F. Shvets, and V. V. Yankov, *Pis'ma Zh. Eksp. Teor. Fiz.* **48**, 79 (1988) [*JETP Lett.* **48**, 83 (1988)].
- [15] J. L. Lebowitz, H. A. Rose, and E. R. Speer, *J. Stat. Phys.* **50**, 657 (1988).

- [16] B. Barviau, J. Garnier, G. Xu, B. Kibler, G. Millot, and A. Picozzi, *Phys. Rev. A* **87**, 035803 (2013).
- [17] P. Suret, S. Randoux, H. R. Jauslin, and A. Picozzi, *Phys. Rev. Lett.* **104**, 054101 (2010); C. Michel, P. Suret, S. Randoux, H. Jauslin, and A. Picozzi, *Opt. Lett.* **35**, 2367 (2010).
- [18] P. Suret, A. Picozzi, and S. Randoux, *Opt. Express* **19**, 17852 (2011).
- [19] S. Iubini, R. Franzosi, R. Livi, G.-L. Oppo, and A. Politi, *New J. Phys.* **15**, 023032 (2013).
- [20] G. Gradenigo, S. Iubini, R. Livi, and S. N. Majumdar, *J. Stat. Mech.* (2021) 023201.
- [21] M. Baldovin, S. Iubini, R. Livi, and A. Vulpiani, *Phys. Rep.* **923**, 1 (2021).
- [22] U. Levy and Y. Silberberg, *Phys. Rev. B* **98**, 060303(R) (2018).
- [23] T. Y. Sheffield and B. Rumpf, *Phys. Rev. E* **95**, 062225 (2017).
- [24] B. Rumpf, A. C. Newell, and V. E. Zakharov, *Phys. Rev. Lett.* **103**, 074502 (2009); A. C. Newell, B. Rumpf, and V. E. Zakharov, *ibid.* **108**, 194502 (2012).
- [25] C. Josserand, Y. Pomeau, and S. Rica, *Phys. Rev. Fluids* **5**, 054607 (2020); B. Rumpf and A. C. Newell, *Phys. Rev. E* **69**, 026306 (2004).